Received: 24 July 2019 | Revised: 9 September 2019 | Accepted: 10 September 2019

DOI: 10.1002/pat.4766

RESEARCH ARTICLE

WILEY polymers advanced technologies

Poly (diallyldimethylammonium) and polyphosphate polyelectrolyte complexes as an all-in-one flame retardant for polypropylene

Lichen Zhang | Deqi Yi | Jianwei Hao

National Engineering Research Center of Flame Retardant Materials, School of Materials Science and Engineering, Beijing Institute of Technology, Beijing 10081, China

Correspondence
Deqi Yi, National Engineering Research Center of Flame Retardant Materials, School of Materials Science and Engineering, Beijing Institute of Technology, No. 5 South Zhongguancun Street, Haidian District, Beijing, 10081, China.
Email: yidq@bit.edu.cn

Funding information
National Natural Science Foundation of China, Grant/Award Number: No. 5130312 5130312

Poly (diallyldimethylammonium chloride) (PDDA) and ammonium polyphosphate (APP) deionized chloride ions and ammonium ions by ionizing in aqueous solution respectively, then combined to form poly (diallyldimethylammonium) and polyphosphate (PAPP) polyelectrolyte complexes as an all-in-one flame retardant for polypropylene and its composites were characterized by Fourier transform infrared (FTIR) spectroscopy and X-ray photoelectron spectroscopy. One flame retardant system composed of PAPP and PP, the other flame retardant system composed of PAPP, Polyamide-6 (PA6) and PP were tested by limiting oxygen index (LOI), UL-94, cone calorimeter tests and thermogravimetric analysis (TGA) and compared with pure PP. The results showed that the LOI value of PP/PAPP composite can reach 27.5%, and UL-94 V-2 rating can be reached at 25 wt% PAPP loading. Meanwhile the cone calorimetry results displayed that the peak heat release rate (PHRR) and total heat release (THR) were reduced up to 69.3% and 22.5%, respectively, compared with those of pure PP. After adding 5 wt% PA6, the carbon source missing due to the early PAPP decomposition can be made up, and PHRR and THR can be further reduced slightly. The flame retardant mechanism of PAPP was studied by FTIR spectroscopy and X-ray photoelectron spectroscopy. Six-membered ring of C—N containing conjugate double bonds, cross-linked phosphate structure formed stable, intumescent, compact char layer which greatly improved the flame retardancy of PP.

KEYWORDS

flame retardance, polyelectrolyte complexes, polypropylene

1 | INTRODUCTION

Polyelectrolyte complexes (PECs) are the result of electrostatic and entropic-driven interactions between oppositely charged polymers or macro-ions in water. The subsequent associative phase separation leads to the formation of a polymer-rich phase that can be either liquid or solid, in equilibrium with a polymer-poor supernatant.[1] Structure of PECs depends on pH, ionic strength, polymer concentration, molar mass, etc. Driving forces for association between oppositely charged biological or synthetic polymers in aqueous solution are enthalpic, entropic, but not electrostatic.[2] Synthetic polyelectrolytes are used in a wide variety of industrial applications such as papermaking,[3,4] wastewater treatment[5] and biomedical materials et al.[6,7] In addition, PECs are widely used in layer-by-layer (LbL) self-assembly technology. Decher et al.[8,9] fabricated free-standing LbL film under physiological condition by using poly (acrylic acid) (PAA)/poly (ethylene oxide) (PEO) as a sacrificial layer and poly (allylaminehydrochloride) (PAH)/poly (sodium-p-styrenesulfonate) (PSSNa) as a top layer. Schlenoff

et al.[10] fabricated free-standing LbL multilayer films based on the salt responsive sacrificial layer (PAA/PDDA). Laufer et al.[11] reported the renewable polyelectrolytes cationic chitosan (CH) and anionic phytic acid (PA), were deposited on cotton fabric via LbL assembly in an effort to reduce flammability. Haile et al.[12] made a water-soluble polyelectrolyte complexes consisting of poly-ethylenimine (PEI) and poly (sodium phosphate) (PSP) to impart flame retardant behavior on cotton fabric. Zhang et al.[13] fabricated a novel PEC originated from positively charged polyethylenimine (PEI) and negatively charged phytic acid (PA) on flame retardant polypropylene. However, apart from Zhang's research works, there are no report about the application of polyelectrolyte complex in flame retardant of thermoplastic materials.

Generally, intumescent flame retardant mainly contains three components, which are acid source, blowing agent, and charring agent. Ammonium polyphosphate (APP) is one of the most important inorganic flame retardants and is chosen as acid source and blowing agent in intumescent flame retardants.[14-16] In addition, APP is also an inorganic polyelectrolyte. While a compound containing an acid source, a gas source, and a carbon source is called "all-in-one" intumescent flame retardant. In detail, deoxyribonucleic acid (DNA) is a "all-in-one" intumescent flame retardant in which the monomeric unit is a nucleotide having three characteristic components: organic nitrogenous bases (adenine (-A-), guanine (-G-), cytosine (-C-) and thymine (-T-)), a pentose unit (deoxyribose), and a phosphate group.[17] DNA had good flame retardant effect when used alone in LDPE.[18]

Poly (diallyldimethylammonium chloride) (PDDA) has a backbone of five-membered cyclic units and highly hydrophilic charged quaternary ammonium groups.[19,20] This special structure provides the polymer with both high water solubility and strong cationic electrolytic solution properties. As a carbon source, PDDA reacted with APP to form polyelectrolyte complexes could be an "all-in-one" intumescent flame retardant system via polyion association.

As we know, the flame-retardant efficiency on PP is quite low when APP is used alone.[21] To achieve the efficient intumescent flame retardancy in polymer, charring agent is necessary to form an expanded char layer during the combustion.[22] Polyamide-6 (PA6) as the charring agent in flame retardant system which played the role of both a polymeric matrix and a carbonization agent because of its unique mechanical properties and processability, it can also improve the mechanical properties of the IFR/PP composites.[23,24] Although extensive research has been contributed to the PECs, the PECs as all-in-one flame retardant are still limited.

In this paper, APP was dissolved in water, act as polyanion, and associated with PDDA polycation by electrostatic interaction to form PAPP (see compound 1, Scheme 1) as an "all-in-one" intumescent flame retardant of polypropylene. Infrared spectroscopy and X-ray photoelectron spectroscopy proved its synthesis successful. The flame retardancy of PAPP/PP composites were investigated using the limiting oxygen index (LOI), UL-94 and cone calorimetry tests (CCT) as well as thermogravimetric analysis (TGA). Compared with pure PP, the flame retardant advantage of polyelectrolyte complex was highlighted, PHRR was reduced by 69.3%, greatly decreasing the risk of fire in real life.

2 | EXPERIMENTAL

2.1 | Materials

Commercial PP (T30S, melt flow rate = 3 g/10 min) was purchased from Daqing Chemical Company. APP with an average degree of polymerization n >1000 was provided by Beijing Institute of Technology Flame Retardant Technology Co. Poly (diallyldimethylammonium chloride) [PDDA; Mw <100,000, average degree of polymerization n < 618, 35 wt% in water] was purchased from Aladdin Reagent Co. Ltd. (China). PA6 (B30S), with a melting point of 227°C and a melt flow index of 110 g/10 min, was obtained from Bayer AG. All of these chemicals were used without further purification.

2.2 | Synthesis of PAPP

0.04 mol of APP and 300 mL of deionized water were added into a 500 mL three-necked flask equipped with a mechanical stirrer. Under vigorous stirring, this solution was heated to 95°C by a thermostatic oil bath. Then 0.04 mol of PDDA, after being dissolved in 100 mL of deionized water, was dropwise added into the APP solution within 1 hr. The reaction was kept at 95°C for 2 hr. Then it was filtered,

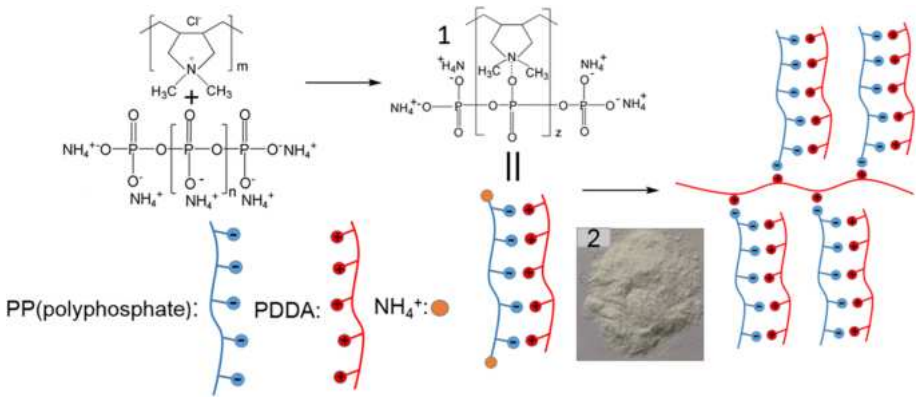

SCHEME 1 Synthesis route of PAPP [Colour figure can be viewed at wileyonlinelibrary.com]

washed by hot deionized water several times, and dried at 90°C overnight. The obtained PAPP was milled and screened through 200 mesh (see picture 2, Scheme 1). The product yield of PAPP was about 77%. The synthesis route of PAPP was shown in Scheme 1. The partial crosslinking structure may be formed due to their different molecular weights.

2.3 | Sample preparation

Composites of PP/PAPP and PP/PAPP/PA6 were meltingblended in a twin-screw extruder (SHJ-20) with a screw length/diameter ratio of 20. The temperatures of the sections were 175°C, 178°C, 182°C, 187°C, 180°C, and 175°C and finally cut into pellets. Samples for testing were molded by means of an injection-molding machine at a temperature profile of 195°C, 190°C, 185°C, 180°C, and 175°C. The formulations of the different PP samples were shown in Table 1.

2.4 | Characterization

Fourier transform infrared (FTIR) spectra were conducted with a Nicolet 6700 IR spectrometer. The spectra were collected through 32 scans with a spectral resolution of 4 cm^{-1} using ATR method.

The elements in FR were examined by X-ray photoelectron spectroscopy (XPS, PHI QUANTERA-II SXM). The binding energy of elements in char residues was characterized by XPS at 15 kV × 25 W under a vacuum lower than 10^{-6} Pa.

The LOI was measured according to ASTMD 2863 with an FTA II oxygen index meter (Rheometric Scientific Ltd., U.K.). The specimens used for the LOI test had dimensions of 118 mm × 6.5 mm × 3 mm.

Vertical burning tests were performed on a CZF-5A-type instrument (Jiangning Analysis Instrument Company, China) according to the UL-94 test standard. The specimens had dimensions of 125 mm × 13 mm × 3.2 mm.

TGA was performed with a NETZSCH 209 F1 thermal analyzer, under a N_2 or air atmosphere at a heating rate of 10°C/min from 40°C to 800°C. The typical results from TGA were reproducible within ±1%, and the reported data are the average of three measurements.

TABLE 1 Formulations of PP samples and their LOI and UL-94 test results

Sample	PP (wt%)	PAPP (wt%)	PA6 (wt%)	LOI (%)	UL-94 Rating
PP	100	--	--	18.0	NR
PP1	95	5	--	20.2	NR
PP2	90	10	--	22.0	NR
PP3	85	15	--	24.4	NR
PP4	80	20	--	26.3	NR
PP5	75	25	--	27.5	V-2
PP6	75	20	5	27.3	V-1

Abbreviations: LOI, limiting oxygen index; PAPP, poly (diallyldimethylammonium) and polyphosphate; PA6, Polyamide-6; PP, polypropylene.

CCT were performed at a heat flux of 50 kW/m^2 according to the ISO 5660 protocol using a Fire Testing Technology apparatus (FTT0007) with a truncated cone-shaped radiator. The specimens (100 mm × 100 mm × 3 mm) were measured horizontally without any grids. Typical results from the cone calorimeter were reproducible within ±10%, and the reported results are the average of three measurements.

Scanning electron microscopy (SEM) experiments were performed with a Hitachi S-4800 scanning electron microscope. Samples (in char analysis section) for SEM were the residue after the CCT and sputtering the surface with Au.

The mechanical properties were measured according to GB/T 1040-2006 (equivalent to ISO 527-2012) with an electronic tensile testing machine (DXLL-5000) at a tensile rate of 20 mm/min. The dimensions of the dumbbell specimens were the same as those specified in GB/T 1040.2-2006.

3 | RESULTS AND DISCUSSION

3.1 | Characterization of PAPP

FTIR spectra of APP, PDDA and PAPP were shown in Figure 1. For APP and PAPP, the absorption bands of P═O, P—O, and P—O—P stretching vibration appeared at 1250 cm^{-1}, 1068 cm^{-1}, and 868 cm^{-1}, respectively.[25] In the FTIR spectrum of APP, the peak at 3162 cm^{-1}, 3000 cm^{-1}, 2832 cm^{-1} and 1422 cm^{-1} were attributed to the typical absorption of NH_4^+, while PAPP didn't exist, indicating that there was almost no NH_4^+ in PAPP. For the spectra of PDDA and PAPP, the characteristic peaks of —OH, —CH, $—CH_3$, $—CH_2$ and C—N of PDDA were 3371–3253 cm^{-1}, 3033 cm^{-1}, 2942 cm^{-1}, 2861 cm^{-1} (stretching vibration), 1471 cm^{-1} (bending vibration) and 1145 cm^{-1}, respectively, and corresponded to the spectra of PAPP. The band at 954 cm^{-1} can be due to $—(CH_2)N^+(CH_3)_2(CH_2)—$ stretching vibration in the FTIR spectrum of PDDA.[26] However, in PAPP this

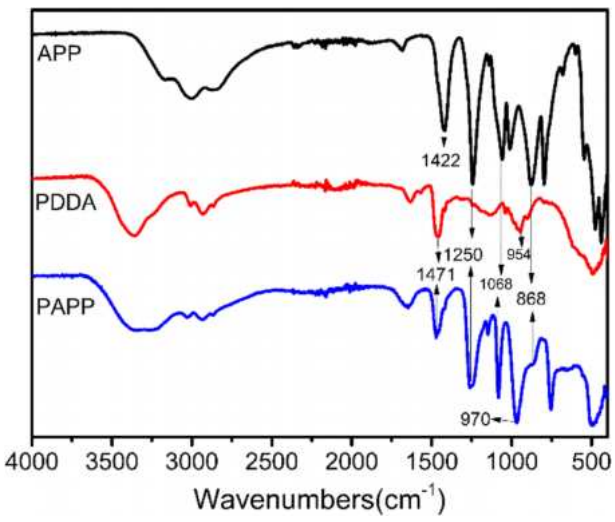

FIGURE 1 FTIR spectra of APP, PDDA and PAPP [Colour figure can be viewed at wileyonlinelibrary.com]

peak blue-shifted to 970 cm^{-1} because the introduction of phosphate groups increased steric hindrance compared to PDDA.

To further confirm the structure of PAPP, XPS was employed to detect the atomic concentration of carbon (C), nitrogen (N), oxygen (O), phosphorus (P) about PAPP and the functional groups of APP, PDDA and PAPP. The XPS spectrum of PAPP was shown in Figure 2 and the element identification of functional groups of PAPP were listed in Table 2. The atomic content of C, N, O, P are 61.4%, 7.6%, 23.5%, 7.5% respectively, which were approximately in accordant with their theoretical value. The XPS high resolution spectra of APP, PDDA and PAPP were shown in Figure 3. In the XPS high resolution spectra of APP, the peaks at 401.5 eV, 531.6 eV, 533.4 eV and 134.1 eV were ascribed to the NH_4^+, P═O, P—O—P and PO_4^{3-}, respectively.[27] The binding peaks at 284.6 eV, 285.9 eV, 401.9 eV and 196.5 eV in the PDDA spectra were assigned to the C—H/C—C, C—N, N^+ and N—Cl, respectively.[28] From the C1s spectrum of PAPP, the peaks at 284.6 eV, 286.0 eV were ascribed to the C—H/C—C, C—N, respectively.[29] In the N1s spectrum of PAPP, the peaks at 399.6 eV and 400.6 eV were assigned to the C—N and N—O, respectively.[30] And the peak of NH_4^+ at 401.5 eV didn't appear. As shown in O1s of PAPP, the peak at 531.6 eV, 532.7 eV and 533.4 eV were assigned to P═O, N—O and P—O—P, respectively. For the P2p spectrum of PAPP, the peak at 134.0 eV was assigned to the PO_4^{3-} group. All of the above results showed that the target polyelectrolyte complexes, PAPP, has been synthesized successfully.

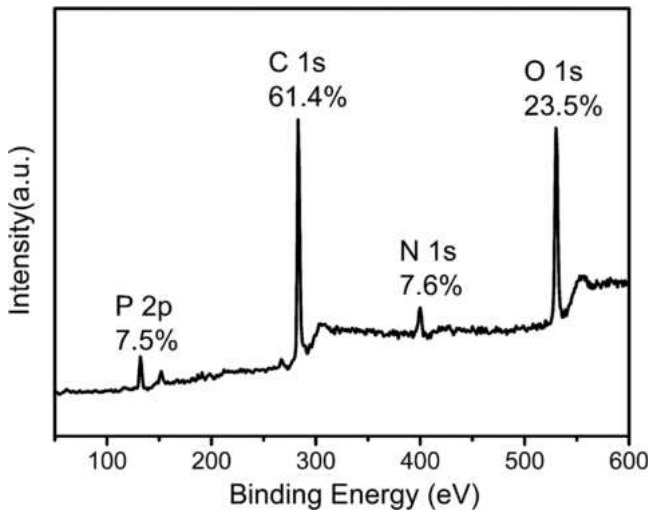

FIGURE 2 XPS spectrum of PAPP

Figure 4 presented the TGA and DTG curves of APP, PDDA and PAPP from room temperature to 800°C. The related data were summarized in Table 3. The initial thermal degradation ($T_{5\ wt\%}$) and maximum weight loss temperatures (T_{max}) of APP were 313.6°C, 588.0°C, respectively, both higher than PAPP which temperature were 302.8°C, 428.4°C. The main decomposition temperature of PDDA and PAPP was in the range of 300–500°C, and APP was in the range of 500–650°C. The thermal decomposing process of APP can be divided into two steps. The first step was in the range of 300–500°C, the weight loss was attributed to the elimination of NH_3 and H_2O during the thermal decomposing process of polyphosphate.[31] The second step was in the range of 500–700°C, this weight loss was attributed to the release of phosphoric acid, polyphosphoric acid, and metaphosphoric acid with APP decomposition.[32] The thermal decomposing process of PDDA can also be divided into two steps. The first stage of PDDA decomposition occurred at 300–400°C, chloride ions were removed, and two methyl groups were broken, with a loss of mass ratio of 41%. The second stage of PDDA decomposition occurred at 400–480°C, with almost complete decomposition. PAPP had only one step thermal decomposition at 300–500°C, releasing hydrocarbon gas to form crosslinked structure of C—N—P and P—O—P. Clearly, PAPP showed a stable degradation between 500°C and 800°C, and its char residue remained about 26.1%. It could form an early and stable char residue, which was beneficial to the protection of PP matrix. As a contrast, the curve of APP started to dramatically decrease above 500°C and showed 15.1% residue at 800°C, the curve of PDDA flattened out above 500°C but only left 1.2% residue at 800°C. In addition, the maximum weight loss rate (MLR) of PAPP was the lowest among those three samples. The above results revealed that PAPP possessed relatively good thermal stability which could meet the processing requirements for PP.

3.2 | Morphologies and mechanical properties of PP composites

The SEM (at magnification of 1000×) images of fracture surfaces of PP5(a), PP6(b) are shown in Figure 5. The samples were frozen in

TABLE 2 Element identification of functional groups of PAPP

	Atomic Concentration (%)			
Element	Experimental Value	Theoretical Value	Binding Energy (eV)	Group
C1s	61.4	61.5	284.6 286.0	C—H and C—C C—N
N1s	7.6	7.7	399.6 400.6	C—N N—O
O1s	23.5	23.1	531.6 532.7 533.4	P═O N—O P—O—P
P2p	7.5	7.7	134.0	PO_4^{3-}

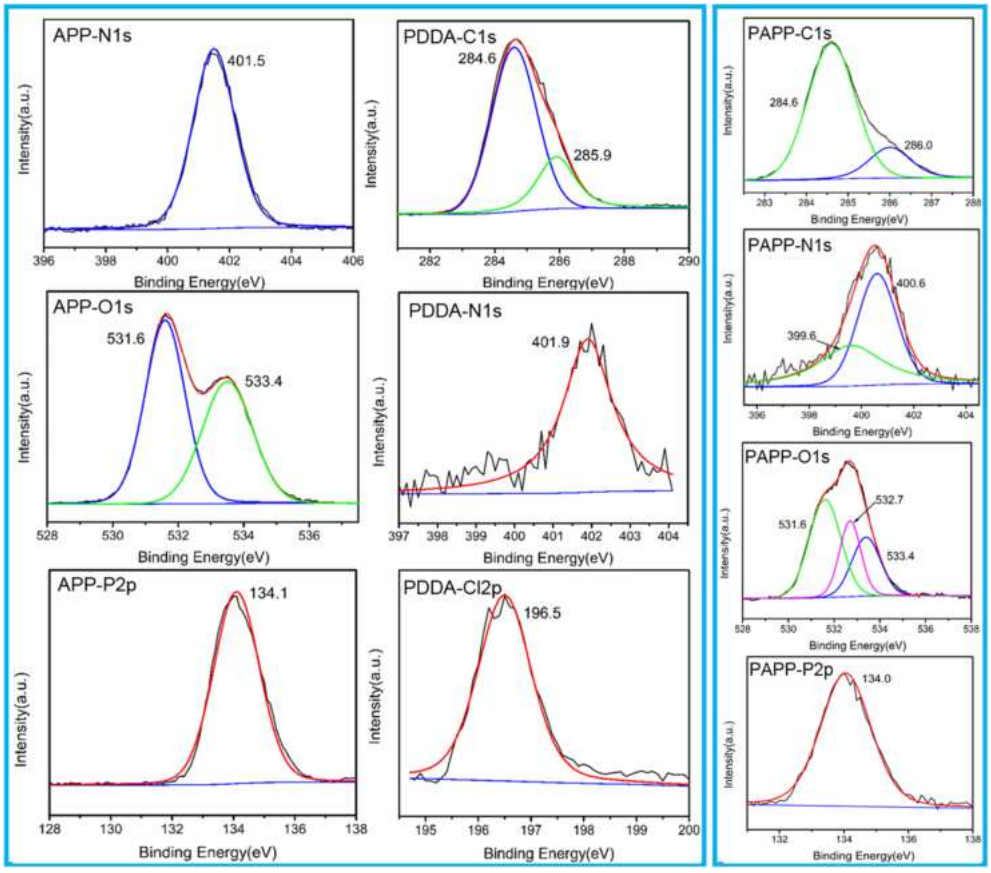

FIGURE 3 The XPS high resolution spectra of APP, PDDA and PAPP [Colour figure can be viewed at wileyonlinelibrary.com]

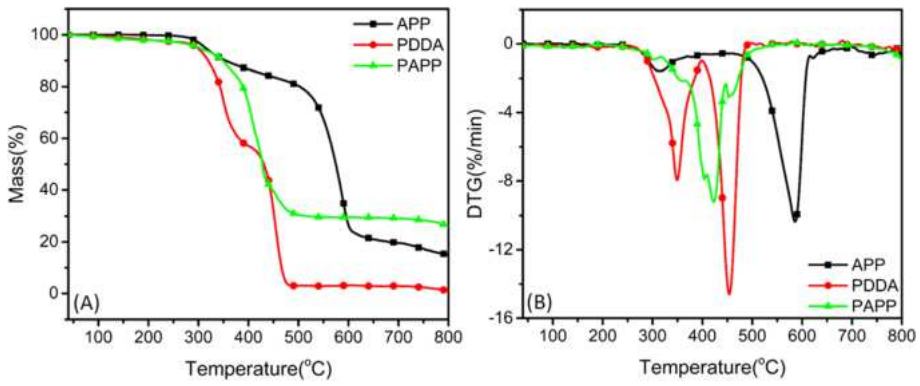

FIGURE 4 TGA (A) and DTG (B) curves of APP, PDDA and PAPP in N_2 atmosphere [Colour figure can be viewed at wileyonlinelibrary.com]

liquid nitrogen for 10 min and then broken off. As can be seen from Figure 5A, there were several large spherical bulges, which should be the aggregates of PAPP. In Figure 5B, the aggregates disappeared and the surface tended to be smooth, which was attributed to the addition of PA6 to increase the compatibility between PAPP and PP.

The mechanical properties of the PP samples were listed in Table 4. The tensile strength, elongation at break and Young's modulus of pure PP were 29.8 MPa, 74.4% and 271.1 MPa, respectively. In the addition of PAPP, PA6, the tensile strength and elongation at break were decreased but Young's modulus were higher compared with pure PP. Although the tensile strength and elongation at break were reduced compared to pure PP with the increasing of flame retardant. The mechanical properties of PP6 were better than PP4 due to the addition of PA6. The above results showed that there was an obvious interface between PAPP and PP, and the addition of a small amount of compatibilizer PA6 can improve the mechanical properties.

3.3 | Thermogravimetric analyses of PP samples

The thermal stabilities of PP, PP composites and PA6 were measured by TGA in N_2 and air atmosphere. The TGA and DTG curves in N_2

TABLE 3 TGA and DTG data of APP, PDDA and PAPP

Sample	$T_{5\ wt\%}$ (°C)	$T_{10\ wt\%}$ (°C)	T_{max} (°C)	MLR (%/min)	CR $_{800°C}$ (wt%)
APP	313.6	354.5	588.0	−10.4	15.1
PDDA	297.1	318.8	454.0	−14.6	1.2
PAPP	302.8	348.6	428.4	−9.2	26.1

Abbreviation: MLR, maximum weight loss rate.

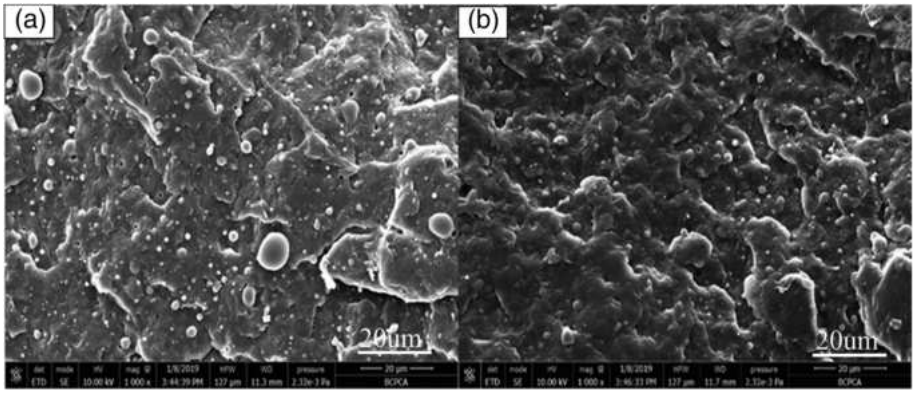

FIGURE 5 SEM images of fracture surfaces of PP5 (A) and PP6 (B)

TABLE 4 Mechanical properties of PP samples

Sample	Tensile Strength (MPa)	Elongation at Break (%)	Young's Modulus (MPa)
PP	29.8 ± 1.2	74.4 ± 7.4	271.1 ± 35.9
PP1	29.2 ± 0.8	63.9 ± 6.8	286.7 ± 33.6
PP2	28.3 ± 0.9	55.5 ± 6.3	292.6 ± 42.2
PP3	26.9 ± 0.8	46.2 ± 5.3	300.2 ± 31.5
PP4	25.8 ± 0.6	38.3 ± 4.5	309.3 ± 32.3
PP5	25.1 ± 0.5	33.7 ± 2.9	318.6 ± 40.4
PP6	26.6 ± 0.7	43.1 ± 3.1	313.4 ± 45.2

atmosphere were shown in Figure 6, and the specific degradation temperatures and the final char yield at 800°C were presented in Table 5. The $T_{5\ wt\%}$ of PP composites were lower than PP because the decomposition of the PAPP ahead of time. Although $T_{5\ wt\%}$ and $T_{10\ wt\%}$ showed a decreasing trend with the increasing of flame retardant, the initial decomposition temperature of PP6 was higher than PP1 with the addition of PA6. Meanwhile, T_{max} and MLR of PP composites were all higher than PP, suggesting that their thermal stabilities were improved. Because of the early decomposition of PAPP, the initial decomposition temperature of PP5 decreased, but the flame retardant system facilitated the formation of the early intumescent char layer, thus protecting the PP matrix. Moreover, a small amount of PA6 could make up for the missing carbon source and made the system have better thermal stability. The experimental (Exp.) TGA curve of PP6 was obtained from TGA test, whereas the calculated (Cal.) curve was obtained according to their weight percentage in the mixture. In addition, all the data of TGA and DTG about PP6-Exp. were more than PP6-Cal., indicating that there are synergistic effect between PAPP and PA6 in PP matrix during thermal degradation.

The TGA and DTG curves of pure PP, PA6, PAPP and PP composites in air atmosphere were shown in Figure 7, and the related data were listed in Table 6. The pyrolysis of PP in air was relatively rapid,

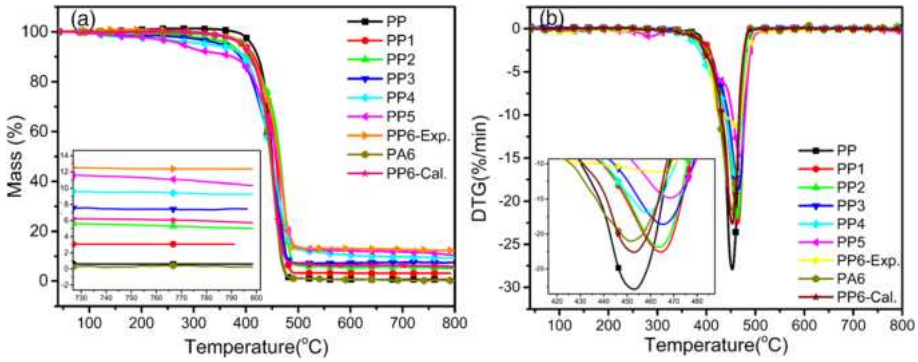

FIGURE 6 TGA (A) and DTG (B) curves of PP, PP composites and PA6 in N_2 atmosphere [Colour figure can be viewed at wileyonlinelibrary.com]

TABLE 5 TGA and DTG data of PP, PP composites and PA6 in N_2 atmosphere

Sample	$T_{5\ wt\%}$ (°C)	$T_{10\ wt\%}$ (°C)	T_{max} (°C)	MLR (%/min)	CR $_{800°C}$ (wt%)
PP	410.9	422.9	454.4	−27.9	0.6
PP1	392.7	414.1	464.3	−22.6	3.1
PP2	368.5	397.5	463.2	−21.9	5.1
PP3	354.7	391.2	465.7	−18.6	7.5
PP4	326.8	383.9	461.7	−16.9	9.3
PP5	310.2	372.6	468.3	−14.8	10.4
PP6-Exp.	394.8	410.5	462.2	−11.2	12.4
PA6	381.6	399.1	441.8	−21.0	0.1
PP6-Cal.	391.0	407.8	452.9	−22.6	5.7

Abbreviation: MLR, maximum weight loss rate.

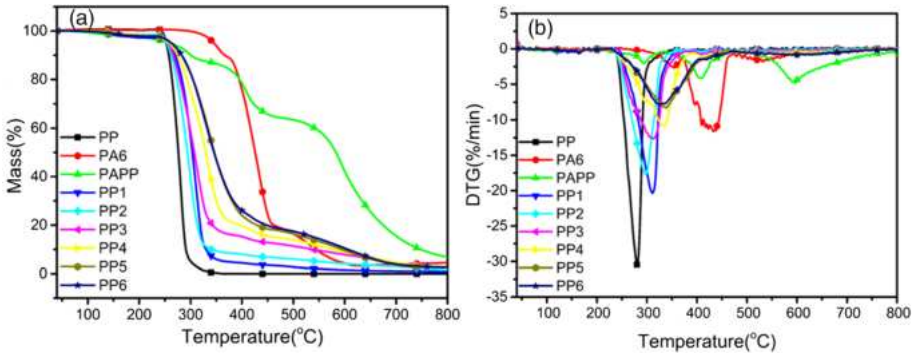

FIGURE 7 TGA (A) and DTG (B) curves of pure PP, PA6, PAPP and PP composites in air atmosphere [Colour figure can be viewed at wileyonlinelibrary.com]

TABLE 6 TGA and DTG data of pure PP, PA6, PAPP and PP composites in air atmosphere

Sample	$T_{5\ wt\%}$ (°C)	$T_{10\ wt\%}$ (°C)	T_{max} (°C)	MLR (%/min)	CR $_{800°C}$ (wt%)
PP	252.8	257.6	280.3	−30.5	0.0
PA6	345.4	366.4	432.8	−11.6	4.4
PAPP	258.7	300.2	596.8	−4.9	6.9
PP1	259.0	270.3	311.1	−20.3	0.9
PP2	254.0	262.3	297.6	−17.7	1.6
PP3	257.1	266.3	312.4	−12.6	2.4
PP4	259.6	274.8	334.1	−10.9	2.5
PP5	262.5	282.4	338.3	−8.3	2.6
PP6	262.8	282.6	325.9	−7.8	2.7

Abbreviation: MLR, maximum weight loss rate.

the $T_{5\ wt\%}$ of PP was 252.8°C, and when it was increased by 100°C to 352.8°C, only 0.31% of residual char remained. The thermal stability of PA6 was much higher than PP, the corresponding data were both better in air atmosphere. PAPP had three decomposition peaks in the air, MLR was only -4.9%/min, and there was still 62 wt% residual char at 500°C, showing good thermal stability. Compared with pure PP, $T_{5\ wt\%}$ and T_{max} of all PP composites shifted to higher temperature and the peaks became broad, residual char increased, indicating PAPP slowed the thermal degradation in air atmosphere.

3.4 | Cone calorimeter tests

The cone calorimeter can simulate the combustion behavior of materials in real fire disasters.[33] The heat release rate (HRR), total heat

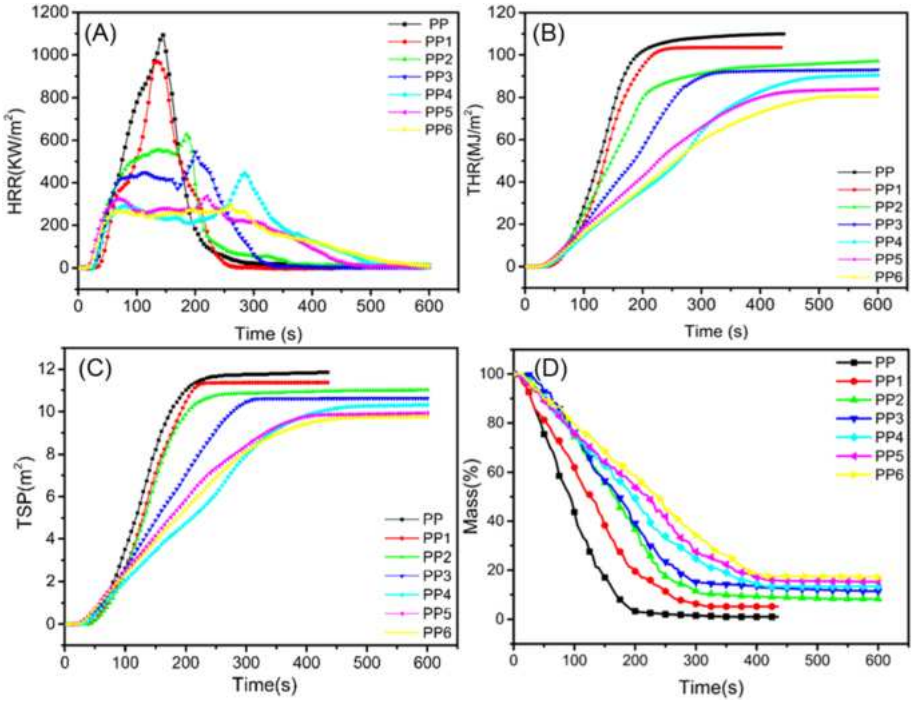

FIGURE 8 CCT results of PP and its composites: (A) HRR, (B) THR, (C) TSP and (D) ML [Colour figure can be viewed at wileyonlinelibrary.com]

TABLE 7 Cone calorimetry tests data of PP and its composites

Sample	TTI (s)	PHRR (kW/m^2)(Reduction %)	t_{PHRR} (s)	THR (MJ/m^2)	TSP (m^2)	Char residue (wt%)	FPI (m^{2}s/kW)	FGI (kW/m^{2}s)
PP	30	1092.7 ± 40.2(—)	145	108.2 ± 4.2	11.8	1.0	0.027	7.54
PP1	28	968.5 ± 34.4(11.4)	135	103.4 ± 3.9	11.4	5.1	0.029	7.17
PP2	25	626.2 ± 32.1(42.7)	185	97.1 ± 2.2	11.0	8.2	0.040	3.38
PP3	23	543.1 ± 23.0(50.3)	200	94.3 ± 2.5	10.6	11.4	0.042	2.71
PP4	21	443.9 ± 19.6(59.4)	285	90.1 ± 3.2	10.3	13.3	0.047	1.56
PP5	18	335.3 ± 15.9(69.3)	220	83.9 ± 1.9	9.9	15.2	0.054	1.52
PP6	17	295.2 ± 16.8(73.0)	265	80.5 ± 1.7	9.7	17.2	0.058	1.11

Abbreviations: FGI, fire growth index; FPI, fire performance index; PHRR, peak heat release rate; THR, total heat release; TSP, total smoke production; TTI, time to ignition.

release (THR), total smoke production (TSP) and mass loss (ML) curves of different specimens were shown in Figure 8, and some important data from the CCT were summarized in Table 7. HRR, especially peak heat release rate (PHRR), is a key parameter obtained from CCT. From Figure 8A and Table 7, it was found that PP burnt very rapidly after being ignited, and a very sharp HRR peak appeared at about 145 s corresponding to the peak of 1092.7 kW/m^2, and its THR is 108.2 MJ/m^2. Obviously, with the increasing of flame retardant, PHRR and THR decreased significantly. The PHRR of PP2 only added with 10 wt% PAPP could reach 626.2 kW/m^2, which was 42.7% less than pure PP. The images of PP4, PP5 and PP6 all had a platform. A sharp peak appeared behind the PP4 platform, and the HRR peak was relatively prominent, indicating that the char layer ruptured in the later period, with the formation of pores, and without the dense char layer, the protective effect cannot be achieved, resulting in a large release of heat and the formation of a higher HRR peak. The flat platforms of PP5 and PP6 had no prominent peaks behind, indicating that their char layers were dense and could form a good shielding effect to reduce the release of heat and protect the underlying materials from further burning. For PP5, the PHRR and THR were decreased to 335.3 kW/m^2 and 107 MJ/m^2, a decrease of 69.3% and 22.5% compared to PP, respectively. Those showed that a good flame retardant effect could be achieved by using 25 wt% PAPP alone. In addition, the PHRR and THR of the PP6 and PP5 samples were substantially similar and slightly reduced. This showed that when PAPP was used as the intumescent flame retardant, the carbon source content was slightly insufficient due to the thermal decomposition of poly (diallyldimethylammonium).

Smoke performance is another important factor to evaluate the fire safety of materials. The TSP and ML curves of PP and PP composites were shown in Figure 8C,D. It can be seen that TSP curves were similar to THR curves, and the peak values of TSP were decreased with

the increasing of PAPP. The TSP of PP5 was decreased to 9.9 m^2 from 11.8 m^2 of PP. With the addition of PA6, the TSP of PP6 was further decreased to 9.7 m^2. Besides, at the end of burning, the char residue of PP, PP5 and PP6 were 1.0 wt%, 15.2 wt% and 17.2 wt%. These results showed that only adding PAPP could also play a role in smoke suppression in condensed phase. After adding a small amount of PA6, a more stable char layer was formed and the flame retardant effect was further improved.

Time to ignition (TTI), fire performance index (FPI), and fire growth index (FGI) were selected to judge the fire hazards of pure PP and the composites.[34] TTI was used to determine the influence on ignitability, which could be measured from the onset of an HRR curve.[35] As shown in Table 6, the TTI of pure PP was 30 s, while other samples all declined. The reason might be that PAPP decomposed at a relatively low temperature and released small volatile molecules, making the sample easier to burn under the radiation of heat flow. The decomposition of PAPP in advance in the combustion process was beneficial to the formation of an expanding protective layer to protect the matrix from further combustion. FPI is defined as the proportion of TTI and PHRR. FGI is defined as the proportion of PHRR and t_{PHRR} (time to PHRR). It is generally accepted that the greater the value of FPI and the smaller the value of FGI correspond to the less fire hazard.[36] Similarly, with the increase of PAPP, FPI was on the rise and FGI was on the decline. The FPI and FGI values of PP5 could achieve good results, greatly reducing the risk of fire.

The digital photographs of the residual chars after CCT are shown in Figure 9. As can be observed from Figure 9A, PP burned out, leaving no char at all. From Figure 9B to Figure 9G, the area and content of residual chars cover gradually increased, and the residual chars became more compact and continuous. Figure 9H,I were the side view of residual chars of PP5 and PP6 to exhibit the intumescent situation of the specimens. These two pictures showed that PP5 and PP6

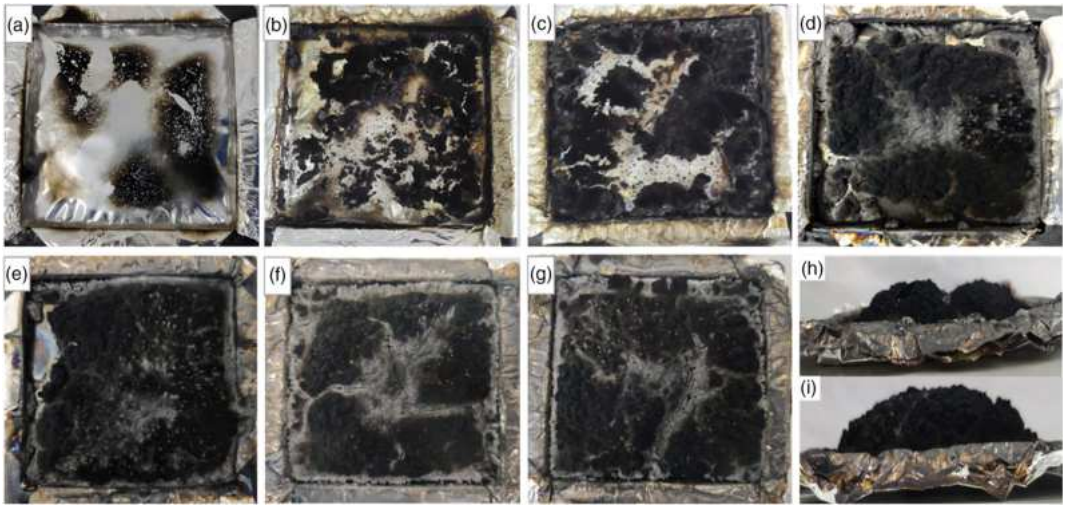

FIGURE 9 Digital photos of residual chars after CCT: (A) PP, (B) PP1, (C) PP2, (D) PP3, (E) PP4, (F, H) PP5 and (G, I) PP6 [Colour figure can be viewed at wileyonlinelibrary.com]

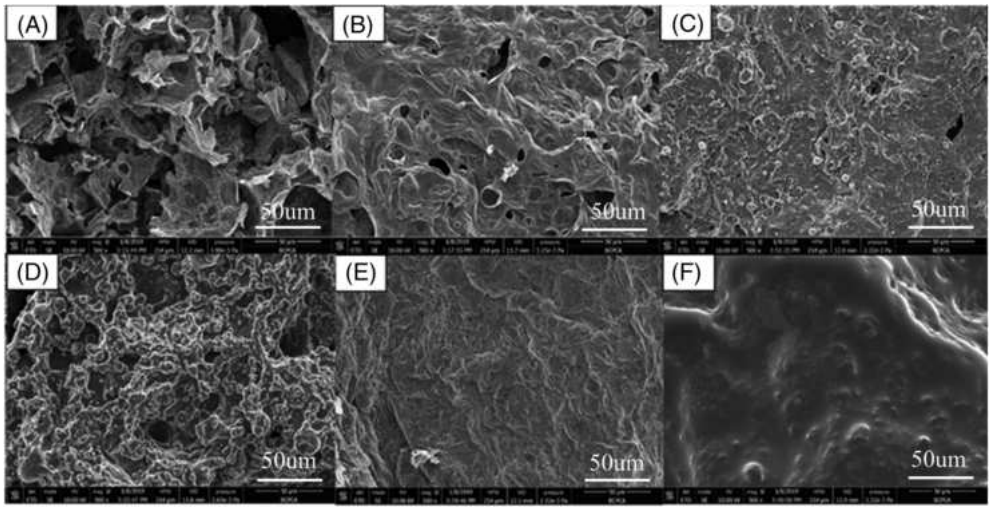

FIGURE 10 SEM micrographs of the char formed after CCT: (A) PP1, (B) PP2, (C) PP3, (D) PP4, (E) PP5 and (F) PP6

formed the thick intumescent char layer after combustion, which was conducive to slowing down the heat and mass transfer and preventing further burning of the substrate.

3.5 | Analysis of the residual char

The morphologies of chars of PP composites after CCT were observed by SEM (at magnification of 500×, as shown in Figure 10). From Figure 10A, there can be observed that a lot of fragments and holes were distributed on the char of PP1 which were disorderly and unsystematic. From PP1 to PP6, the surface of char became more and more flat with fewer holes. Holes appeared on the surface of char layer of PP4, and flammable gas could be released from the holes. The surface of char layer of PP5 and PP6 were complete and dense, which could play a good blocking role. These matched HRR images from PP4, PP5, and PP6. For PP5 and PP6, the better quality of char meant the better barrier effect. Through suppressing the spread of combustible radicals and heat in the process of combustion, the char of PP5 and PP6 played the role of barrier, enhancing the flame retardancy of composite.[37,38] In addition, the smooth char layer of PP6 indicated good fluidity and low viscosity of the flame retardant system,[39] which may lead to melt dripping.

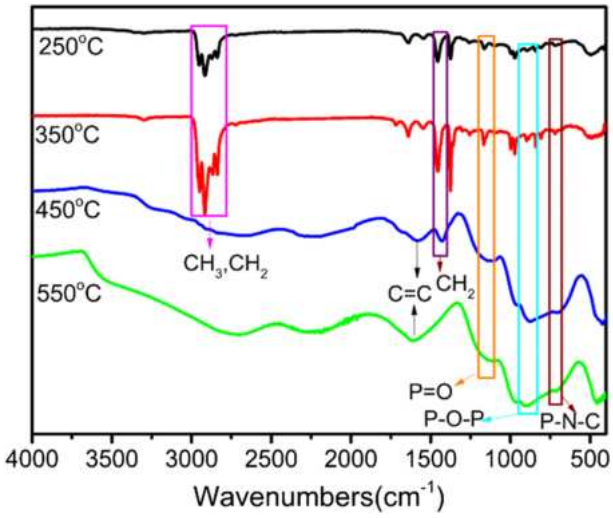

FIGURE 11 The real time FTIR spectra of PP5 composite residue at different pyrolysis temperature [Colour figure can be viewed at wileyonlinelibrary.com]

To obtain a deeper understanding of the flame-retardant behavior of the PAPP/PP system, the chemical structures of the residues obtained at different treating temperature were analyzed by using FTIR. The FTIR spectra of heat-treated sample at 250°C, 350°C, 450°C, and 550°C was shown in Figure 11. It can be seen from Figure 11 for PP/PAPP composite at 350°C, the peaks appear at 2917 cm^{-1} and 2865 cm^{-1} corresponding to the stretching vibration of methyl and methylene groups, the peaks at 1457 cm^{-1} and 1375 cm^{-1} ascribed to the bending vibration of methylene and methyl groups. The absorption bands at around 1375 cm^{-1} (—CH_3) and 2800–3000 cm^{-1} disappeared at 450°C, demonstrating that —CH_3 vanished in the process of decomposition. However, the absorbing peak of —CH_2— at 1457 cm^{-1} still existed at 450°C, and the absorbing peak at 1626 cm^{-1} became wider, indicating the existence of structures containing C═C. For PP5, the absorption peaks between 1150

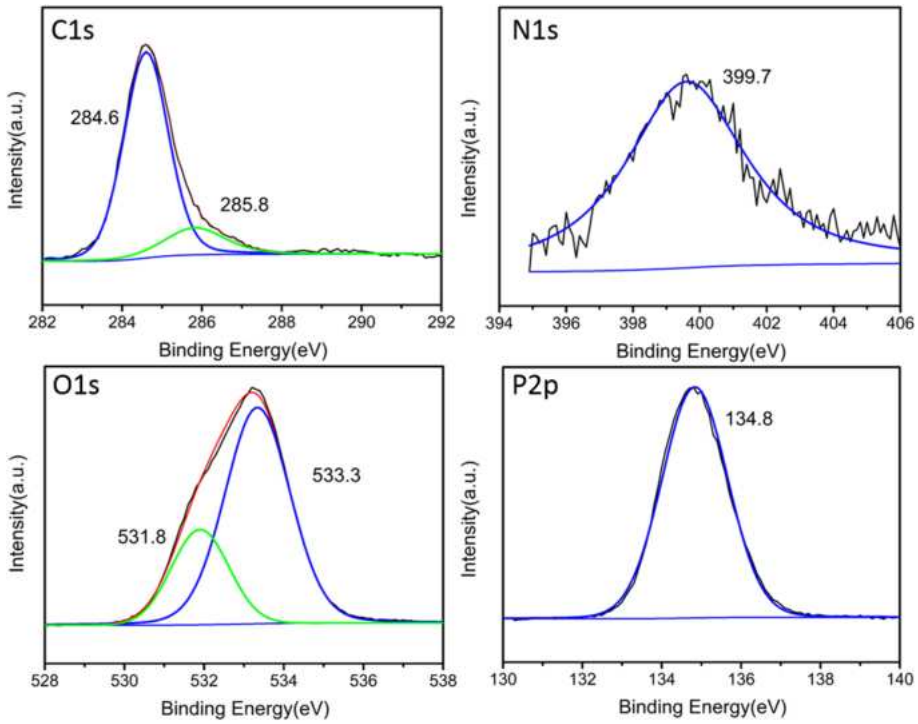

FIGURE 12 The X-ray photoelectron spectroscopy (XPS) curves of C1s, N1s, O1s and P2p of the char formed after CCT about PP5 [Colour figure can be viewed at wileyonlinelibrary.com]

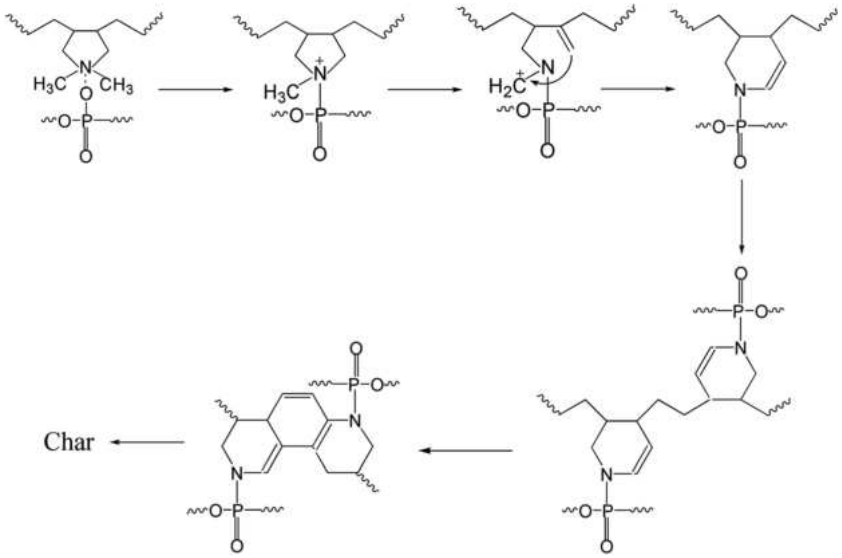

SCHEME 2 Charring mechanism of PAPP during the combustion process

$cm^{-1}$and 1250 cm^{-1} attributed to the stretching vibration of P═O, the peaks for P—O—P at around 900–1000 cm^{-1} still existed at 550°C, indicating the existence of phosphate in the condensed phase. For Figure 10, the peak of P—N—C was observed at 723 cm^{-1} during increasing the temperature from 250°C to 550°C. It was well established that the P—N—C rich char residue could further form the stable residual char, resulting in better flame retardancy.[40]

To further investigate the chemical composition and interactions in the char of PP/PAPP composite, the sample was studied by XPS, and the results were presented in Figure 12. In the C1s spectra of PP5, by curve fitting treatment, two characteristic peaks at 284.6 eV and 285.8 eV were emerged, which were corresponding to C—C, C—H, C═C and C—N bonding respectively. This proved that the hybridization mode of C in the char was sp^2. It was clearly seen that only one peak at 399.7 eV (assigned to C—N) in N1s spectra. The O1s spectrum had two distinct peaks with binding energy at 531.8 eV (assigned to P═O), 533.3 eV (P—O—P). Besides, the peak at 134.8 eV in P2p spectrum was attributed to PO_3^-.

According to the FTIR and XPS tests results, the possible charring mechanism for PP5 during the combustion was figured out as shown in Scheme 2. As PP didn't take part in the charring reaction, it didn't appear in the mechanism. In the early stage, CO_2 and H_2O were released along with the breakdown of one methyl group,[41] and P—N—C structure was formed in the combustion process, which was conducive to the formation of a relatively stable primary char residue. And then Hofmann elimination reaction occurred, generating C═C,[42] methyl group was removed one molecule of H, formed carbenium ion and rearranged with double bond to form C—N six-membered ring.[43] As the temperature was further increased, H^+ was removed from the main chain to form a stable six-membered ring structure. PAPP formed P—N—C, C═C, cross-linked phosphate structure, six-membered ring of C—N containing conjugate double bonds after combustion, respectively. These structures promoted the formation of stable, expanding, dense char layer, and the excellent flame retardant performance of PP composites was achieved. Otherwise, the addition of a small amount of PA6 increased the char forming ability of the system.[44]

3.6 | LOI and UL-94 tests

LOI and vertical burning tests were used to evaluate the flame retardant property of PP composites, and the data was listed in Table 2. PP is a flammable polymer with LOI at only 18%. With the linear increase of PAPP, the LOI value of PP composite increased approximately linearly. In the addition of PAPP and PA6, the UL-94 V-1 rating can be reached at 25% FR loading, and the composite's LOI could reach 27.3%. The LOI value of PP5 with the same content of PAPP was the maximum value of 27.5%, and UL-94 was V-2, which was due to the low viscosity of the system and the droplet generated in the combustion process, extending the extinguishing time. In the future, only anti-melt drops need to be added to increase the viscosity of the system, and the vertical combustion performance can be improved, but this is not the focus of this paper.

4 | CONCLUIONS

A new all-in-one flame retardant polyelectrolyte complexes (PAPP) was successfully synthesized, and applied it as a flame retardant to polypropylene for the first time. The UL-94 vertical burning, LOI and CCT demonstrated that PAPP had a good flame retardant performance for PP. PP/PAPP composite could pass the UL-94 V-2 rating (3.2 mm) at 25 wt% flame retardant. Meanwhile, its LOI value might reach 27.5%. For combustion performance, the cone calorimetry results displayed that the PHRR and THR of IFR were reduced up to 69.3% and 22.5%, respectively, compared with pure PP. PA6 played an important role in increasing mechanical properties and charring ability, a small amount of PA6 could increase the compatibility of the system and made up for the carbon source missing in the earlier stage due to decomposition. P—N—C, six-membered ring of C—N containing

conjugate double bonds and cross-linked phosphate structure were formed during the combustion process, which led to stable, intumescent, compact char layer. Finally, this work demonstrated a new polyelectrolyte complexes as flame retardant, which would have promising applications to various polymer-based materials.

ACKNOWLEDGEMENT

The work was partially supported by the National Natural Science Foundation of China (No. 5130312).

NOTES

The author declare no competing financial interest.

ORCID

Deqi Yi https://orcid.org/0000-0001-5603-876X

REFERENCES

1. Liu Y, Momani B, Winter HH, Perry SL. Rheological characterization of liquid-to-solid transitions in bulk polyelectrolyte complexes. *Soft Matter*. 2017;13(40):7332-7340.
2. Fu J, Schlenoff JB. Driving forces for oppositely charged polyion association in aqueous solutions: enthalpic, entropic, but not electrostatic. *J Am Chem Soc*. 2016;138(3):980-990.
3. Korhonen MHJ, Laine J. Flocculation and retention of fillers with nanocelluloses. *Nord Pulp Pap Res J*. 2014;29(1):119-128.
4. Schnell CN, Tarrés Q, Galván MV, et al. Polyelectrolyte complexes for assisting the application of lignocellulosic micro/nanofibers in papermaking. *Cellul*. 2018;25(10):6083-6092.
5. Xu Y, Jia J, Zhong D, Wang Y. Degradation of dye wastewater in a thin-film photoelectrocatalytic (PEC) reactor with slant-placed TiO2/Ti anode. *Chem Eng J*. 2009;150(2-3):302-307.
6. Jayakumar R, Prabaharan M, Nair SV, Tamura H. Novel chitin and chitosan nanofibers in biomedical applications. *Biotechnol Adv*. 2010;28 (1):142-150.
7. Lankalapalli S, Kolapalli VRM. Polyelectrolyte complexes: a review of their applicability in drug delivery technology. *Indian J Pharm Sci*. 2009;71(5):481-487.
8. Ono SS, Decher G. Preparation of ultrathin self-standing polyelectrolyte multilayer membranes at physiological conditions using pH-responsive film segments as sacrificial layers. *Nano Lett*. 2006;6 (4):592-598.
9. Zhao Q, Qian J, An Q, Du B. Speedy fabrication of free-standing layer-by-layer multilayer films by using polyelectrolyte complex particles as building blocks. *J Mater Chem*. 2009;19(44):8448-8455.
10. Jaber JA, Schlenoff JB. Mechanical properties of reversibly cross-linked ultrathin polyelectrolyte complexes. *J Am Chem Soc*. 2006;128 (9):2940-2947.
11. Laufer G, Kirkland C, Morgan AB, Grunlan JC. Intumescent multilayer nanocoating, made with renewable polyelectrolytes, for flame-retardant cotton. *Biomacromolecules*. 2012;13(9):2843-2848.
12. Haile M, Fincher C, Fomete S, Grunlan JC. Water-soluble polyelectrolyte complexes that extinguish fire on cotton fabric when deposited as pH-cured nanocoating. *Polym Degrad Stab*. 2015;114:60-64.
13. Zhang T, Yan H, Shen L, et al. A phosphorus-, nitrogen- and carbon-containing polyelectrolyte complex: preparation, characterization and its flame retardant performance on polypropylene. *RSC Adv*. 2014;4 (89):48285-48292.
14. Bourbigot S, Bras ML, Duquesne S, Rochery M. Recent advances for intumescent polymers. *Macromol Mater Eng*. 2004;289:499-511.
15. Camino G, Costa L, Luda MP. Mechanistic aspects of intumescent fire retardant systems. *Macromol Symp*. 1993;74(1):71-83.
16. Yi D, Yang R. Ammonium polyphosphate/montmorillonite nanocompounds in polypropylene. *J Appl Polym Sci*. 2010;118 (2):834-840.
17. Alongi J, Di Blasio A, Milnes J, et al. Thermal degradation of DNA, an all-in-one natural intumescent flame retardant. *Polym Degrad Stab*. 2015;113:110-118.
18. Isarov SA, Lee PW, Towslee JH, et al. DNA as a flame retardant additive for low-density polyethylene. *Polymer*. 2016;97:504-514.
19. Jing R, Hongfei H. Study on interpenetrating polymer network hydrogel of diallyldimethylammonium chloride with kappa-carrageenan by UV irradiation. *Eur Polym J*. 2001;37(12):2413-2417.
20. Zhao Q, Sun J, Chen S, Zhou Q. Properties of a poly (acrylamide-co-diallyl dimethyl ammonium chloride) hydrogel synthesized in a water-ionic liquid binary system. *J Appl Polym Sci*. 2010;115(5):2940-2945.
21. Almeras X, Le Bras M, Hornsby P, et al. Effect of fillers on the fire retardancy of intumescent polypropylene compounds. *Polym Degrad Stab*. 2003;82(2):325-331.
22. Shao ZB, Deng C, Tan Y, Chen MJ, Chen L, Wang YZ. An efficient mono-component polymeric intumescent flame retardant for polypropylene: preparation and application. *ACS Appl Mater Interfaces*. 2014;6 (10):7363-7370.
23. Chen M, Tang M, Ma Y, et al. Influence of polyamide 6 as a charring agent on the flame retardancy, thermal, and mechanical properties of polypropylene composites. *Polym Eng Sci*. 2015;55(6):1355-1360.
24. Tang Y, Hu Y, Xiao J, Wang J, Song L, Fan W. PA-6 and EVA alloy/clay nanocomposites as char forming agents in poly (propylene) intumescent formulations. *Polym Adv Technol*. 2005;16(4):338-343.
25. Zhang S, Ji W, Han Y, Gu X, Li H, Sun J. Flame-retardant expandable polystyrene foams coated with ethanediol-modified melamine-formaldehyde resin and microencapsulated ammonium polyphosphate. *J Appl Polym Sci*. 2018;135(28):46471.
26. Li M, Li MY, Zhu W, et al. Preparation of cationic polyvinylpyrrolidone and its loading property to RNA. *Chin J Appl Chem*. 2014;31 (6):649-653.
27. Xu Z, Chu Z, Yan L, Chen H, Jia H, Tang W. Effect of chicken eggshell on the flame-retardant and smoke suppression properties of an epoxy-based traditional APP-PER-MEL system. *Polym Compos*. 2018.
28. Zhang J, Jiang J, Zhao X. Synthesis and capacitive properties of manganese oxide nanosheets dispersed on functionalized graphene sheets. *J Phys Chem C*. 2011;115(14):6448-6454.
29. Wang P, Xia L, Jian R, et al. Flame-retarding epoxy resin with an efficient P/N/S-containing flame retardant: preparation, thermal stability, and flame retardance. *Polym Degrad Stab*. 2018;149:69-77.
30. Tourabi M, Nohair K, Traisnel M, Jama C, Bentiss F. Electrochemical and XPS studies of the corrosion inhibition of carbon steel in hydrochloric acid pickling solutions by 3,5-bis(2-thienylmethyl)-4-amino-1,2,4-triazole. *Corros Sci*. 2013;75:123-133.
31. Liu G, Chen W, Yu J. A novel process to prepare ammonium polyphosphate with crystalline form II and its comparison with melamine polyphosphate. *Ind Eng Chem Res*. 2010;49(23):12148-12155.
32. J-w G, G-c Z, S-l D, Q-y Z, Kong J. Study on preparation and fire-retardant mechanism analysis of intumescent flame-retardant coatings. *Surf Coat Technol*. 2007;201(18):7835-7841.

33. Zhao W, Liu J, Peng H, Liao J, Wang X. Synthesis of a novel PEPA-substituted polyphosphoramide with high char residues and its performance as an intumescent flame retardant for epoxy resins. *Polym Degrad Stab*. 2015;118:120-129.

34. Li J, Ke C, Xu L, Wang Y. Synergistic effect between a hyperbranched charring agent and ammonium polyphosphate on the intumescent flame retardance of acrylonitrile-butadiene-styrene polymer. *Polym Degrad Stab*. 2012;97(7):1107-1113.

35. Chen X, Gu A, Liang G, Yuan L, Zhuo D, J-t H. Novel low phosphorus-content bismaleimide resin system with outstanding flame retardancy and low dielectric loss. *Polym Degrad Stab*. 2012;97(5):698-706.

36. Ye X, Wang Y, Zhao Z, Yan H. A novel hyperbranched poly (phosphorodiamidate) with high expansion degree and carbonization efficiency used for improving flame retardancy of APP/PP composites. *Polym Degrad Stab*. 2017;142:29-41.

37. Dong X, Qin R, Nie S, Yang J, Zhang C, Wu W. Fire hazard suppression of intumescent flame retardant polypropylene based on a novel Ni-containing char-forming agent. *Polym Adv Technol*. 2019;30 (3):563-572.

38. Nie S, Hu Y, Song L, He S, Yang D. Study on a novel and efficient flame retardant synergist–nanoporous nickel phosphates VSB-1 with intumescent flame retardants in polypropylene. *Polym Adv Technol*. 2008;19(6):489-495.

39. Zhao M, Yi D, Camino G, Frache A, Yang R. Interdigitated crystalline MMT–MCA in polyamide 6. *RSC Adv*. 2017;7(2):861-869.

40. Shao Z-B, Deng C, Tan Y, Chen M-J, Chen L, Wang Y-Z. Flame retardation of polypropylene via a novel intumescent flame retardant: ethylenediamine-modified ammonium polyphosphate. *Polym Degrad Stab*. 2014;106:88-96.

41. Francis S, Varshney L, Sabharwal S. Thermal degradation behavior of radiation synthesized polydiallyldimethylammonium chloride. *Eur Polym J*. 2007;43(6):2525-2531.

42. Zhu J, Morgan AB, Lamelas FJ, Wilkie CA. Fire properties of polystyrene–clay nanocomposites. *Chem Mater*. 2001;13(10):3774-3780.

43. Mayr H. CC Bond formation by addition of carbenium ions to alkenes: kinetics and mechanism. *Angew Chem Int Ed*. 1990;29(12):1371-1384.

44. Levchik SV, Camino G, Costa L, Levchik GF. Mechanism of action of phosphorus-based flame retardants in nylon 6. I. Ammonium polyphosphate. *Fire Mater*. 1995;19(1):1-10.

How to cite this article: Zhang L, Yi D, Hao J. Poly (diallyldimethylammonium) and polyphosphate polyelectrolyte complexes as an all-in-one flame retardant for polypropylene. *Polym Adv Technol*. 2020;31:260–272. https://doi.org/10.1002/pat.4766